

RESEARCH

Open Access



Surface-functionalized UIO-66-NH₂ for dual-drug delivery of vancomycin and amikacin against vancomycin-resistant *Staphylococcus aureus*

Nazanin Rahmanian¹, Pooria Moulavi², Fatemeh Ashrafi², Aram Sharifi³ and Sepideh Asadi^{4*}

Abstract

Background Conventional antibacterial compounds can inhibit the growth of microorganisms, but their adverse effects and the development of drug limit their widespread use. The current study aimed to synthesize PEG-coated UIO-66-NH₂ nanoparticles loaded with vancomycin and amikacin (VAN/AMK-UIO-66-NH₂@PEG) and evaluate their antibacterial and anti-biofilm activities against vancomycin-resistant *Staphylococcus aureus* (VRSA) clinical isolates.

Methods The VAN/AMK-UIO-66-NH₂@PEG were characterized using scanning electron microscopy (SEM), transmission electron microscopy (TEM), and dynamic light scattering (DLS) to determine their size, polydispersity index (PDI), encapsulation efficiency (EE%), zeta-potential, drug release profile, and physical stability. Antibacterial activity was evaluated using minimum inhibitory concentration (MIC), minimum bactericidal concentration (MBC), and time-kill assays. Biofilm formation by VRSA was assessed using the crystal violet (CV) and minimum biofilm eradication concentration (MBEC) assays. The effect of sub-MIC concentrations of the formulations on the expression of biofilm-related genes (*icaA*, *icaD*) and resistance-related genes (*mecA*, *vanA*) was investigated using quantitative real-time polymerase chain reaction (RT-qPCR).

Results As demonstrated by MIC, MBC and time-kill assay, the VAN/AMK-UIO-66-NH₂@PEG nanoparticles exhibited enhanced antibacterial activity against VRSA isolates compared to free drugs and prepared formulations. Furthermore, CV and MBEC tests indicated that the VAN/AMK-UIO-66@NH₂/PEG can reduce biofilm formation dramatically compared to VAN/AMK and VAN/AMK-UIO-66@NH₂, due to its great drug release properties. This study also found that the expression level of the *mecA*, *vanA*, *icaA*, and *icaD* genes in VAN/AMK-UIO-66@NH₂/PEG treated VRSA isolates was substantially decreased compared to other groups.

Conclusions These findings highlighted the efficiency of VAN/AMK-UIO-66@NH₂/PEG in combating antimicrobial resistance and biofilm formation in VRSA isolates. Future studies, particularly *in vivo* models, are necessary to evaluate the safety, efficacy, and clinical applicability of these nanoparticles for the treatment of bacterial infections.

Keywords Vancomycin-resistant *S. Aureus*, Metal-Organic frameworks, Biofilms, Vancomycin, Amikacin

*Correspondence:

Sepideh Asadi
sepidehasadi1394@yahoo.com

Full list of author information is available at the end of the article



© The Author(s) 2024. **Open Access** This article is licensed under a Creative Commons Attribution-NonCommercial-NoDerivatives 4.0 International License, which permits any non-commercial use, sharing, distribution and reproduction in any medium or format, as long as you give appropriate credit to the original author(s) and the source, provide a link to the Creative Commons licence, and indicate if you modified the licensed material. You do not have permission under this licence to share adapted material derived from this article or parts of it. The images or other third party material in this article are included in the article's Creative Commons licence, unless indicated otherwise in a credit line to the material. If material is not included in the article's Creative Commons licence and your intended use is not permitted by statutory regulation or exceeds the permitted use, you will need to obtain permission directly from the copyright holder. To view a copy of this licence, visit <http://creativecommons.org/licenses/by-nc-nd/4.0/>.

Introduction

Staphylococcus aureus (*S. aureus*) is capable of causing diseases in humans and is also found naturally in the human body. *S. aureus* is responsible for a range of diseases, including infections in the skin and deep tissues, urinary tract infections (UTIs), bacterial conjunctivitis, osteomyelitis, infections acquired in healthcare settings, and infections related to medical implants [1, 2]. It remains a significant public health concern due to the development and spread of strains resistant to multiple drugs [3, 4]. The spread of methicillin-resistant *S. aureus* (MRSA) in developing nations has posed a significant challenge in administering antibiotic therapy and managing severe *S. aureus* infections [1]. The resistance of MRSA strains to beta-lactam drugs is associated with the presence of transportable bacterial genomic islands known as staphylococcal chromosomal cassette mec (SCCmec) [5]. The *mec* gene is responsible for conferring methicillin resistance. The islands undergo fast evolution and consist of various genetic components, including *mecA*, *mecB*, *mecC*, and others [6]. These genes are associated not only to methicillin resistance in *S. aureus* but also to resistance to other categories of antibiotics, including macrolides, lincosamides, streptogramins B, tetracyclines, and aminoglycosides. Vancomycin, a long-established antibiotic, kills bacteria by disrupting their ability to build cell walls. Bacterial membranes are often covered by a cell wall structure that protects the cells from swelling and breaking due to excessive osmolarity inside the cell [7]. Nevertheless, the regular use of vancomycin as a preliminary therapy might quickly lead to the development of vancomycin-intermediate *S. aureus* (VISA) and vancomycin-resistant *S. aureus* (VRSA) [8]. The development of resistance to vancomycin in *S. aureus* is caused by the transfer of the *vanA* operon from *Enterococcus* spp., which is transported by transposon Tn1546 [9]. The *vanA* gene encodes a ligase that modifies the dipeptide residue, significantly reducing the antibiotic's binding ability. This leads to the drug's ineffectiveness against the isolates, making them resistant [9].

In addition, semisynthetic aminoglycosides were developed to combat resistance produced by various aminoglycoside-modifying enzymes. Amikacin is a highly effective semisynthetic aminoglycoside used to treat a range of severe infections caused by Gram-positive and aerobic Gram-negative bacteria [10, 11]. A limited quantity of 6'-N-acetyltransferases exhibiting the AAC(6')-I profile were discovered in Gram-positive bacteria. The AAC(6')-Ie enzyme is connected to the N-terminal end of the phosphotransferase APH(2'')-Ia, forming a dual-function enzyme encoded by the *aac(6')-Ie-aph(2'')-Ia* fusion gene, which is often found within Tn4001-like transposons in Gram-positive bacteria [12]. This gene

confers resistance to aminoglycoside antibiotics, particularly amikacin, in Gram-positive bacteria [13].

A biofilm is a structured community of bacteria that forms a membrane-like extracellular matrix (ECM) by adhering to microbial colonies and secreting extracellular polymeric substances (EPS), including polysaccharides, nucleic acids, and proteins, throughout the development process [14]. The biofilm serves as a protective shield that creates a suitable internal environment for bacterial cell behavior [15]. It protects bacterial cells against unfavorable conditions such as severe temperature, limited nutrient availability, dehydration, and even antibacterial medications. The synthesis of polysaccharide intercellular adhesion (PIA) is controlled by proteins expressed by the *icaADBC* operon in the *ica* locus, which regulates the biofilm formation process in *S. aureus* [16]. The *icaA* and *icaD* genes play a crucial role in regulating biofilm production through this mechanism. The *icaA* gene produces a transmembrane protein known as N-acetylglucosamine transferase [17]. The *icaD* gene produces the chaperone protein for *icaA*. It ensures the proper folding of *icaA* and enhances its selectivity for polymers [18]. The *icaADBC*-mediated synthesis of polysaccharides is a crucial process for creating biofilms and plays a role in the initial proliferation of bacteria [18].

Conventional antibacterial compounds can inhibit the growth of microorganisms, but their adverse effects and the development of drug resistance limit their wider application. Therefore, it is essential to explore novel antibacterial agents. Metal-organic frameworks (MOFs), also known as metal-organic, coordinate polymers or organic-inorganic hybrid materials, have been identified as effective antibacterial agents. MOFs are porous materials with regular network topologies formed by self-assembling metal ions or clusters and organic molecules via coordination bonds [19]. The MOFs possess a high surface area to volume ratio and include metal particles, which makes them advantageous for developing new bactericidal materials with superior efficacy [20]. UIO-66 is a metal-organic framework composed of zirconium ions (Zr⁴⁺). It has a higher drug-loading capacity when compared to commonly used drug delivery carriers such as liposomes and polymers [21]. In their study, Zhu et al., (2014) successfully incorporated the amino bisphosphonate medication Alendronate (AL) into UIO-66 to treat bone cancer. They achieved a high drug loading capacity of 51.4 wt% in the resulting Al-UIO-66 compound [22]. Cunha et al., (2013) discovered that caffeine could be effectively loaded into UIO-66 and exhibited a slow-release capability over 24 h [23]. Yan et al., (2022) used fumaric acid as the ligand for Zr-MOF and observed significant antibacterial activity against Gram-positive *S. aureus* and Gram-negative *E. coli* [24]. Furthermore, PEGylation refers to attaching PEG (poly-ethylene glycol), a non-irritating and

inert hydrophilic polymer, to the surface of nanoparticles [25]. The PEG chains act as steric inhibitors, preventing plasma proteins from binding and thereby enhancing the long-term stability of nano-drug delivery systems. Additionally, PEGylation improves the pharmacokinetics, bio-distribution, and retention of nano-vehicles at the target site, increasing therapeutic efficacy by achieving a higher drug concentration [26].

The aim of this study is to develop an innovative dual drug delivery system targeting vancomycin-resistant *Staphylococcus aureus* (VRSA) infections. We propose the design of biological interfaces by combining UIO-66-NH₂ with PEG polymer to enhance the delivery of vancomycin (VAN) and amikacin (AMK). By utilizing these two antibiotics, which are known for their efficacy against Gram-positive bacteria, we aim to reduce the required antibiotic doses while maintaining antibacterial effectiveness. This dual delivery approach holds promise for improving treatment outcomes in patients facing multidrug-resistant infections.

Materials and methods

Loading of vancomycin and amikacin into the UIO-66-NH₂@PEG

A solution for synthesizing UIO-66-NH₂ was prepared by dissolving 0.41 g of 2-amino terephthalic acid (purchased from Sigma-Aldrich, Germany) and 0.54 g of ZrCl₄ in 31 mL of DMF at 25 °C. The mixture was consistently stirred until a transparent solution was obtained. The solution was then transferred to a Teflon-coated hydrothermal autoclave and heated at 120 °C for 24 h. It was then cooled back down to the surrounding temperature. The resultant particles were centrifuged three times and subjected to ultrasonic treatment in DMF and chloroform for 15 min to replace DMF and remove any unreacted materials. Five days after the initial preparation, the UIO-66 sample underwent a solvent exchange process. This involved daily sonication of the sample for 15 min, fully submerged in 15 mL of fresh chloroform, for five consecutive days. The nanoparticles were then pressure dried at 120 °C to eliminate any remaining solvents.

To integrate VAN and AMK (both from EXIR Company, Iran) into the UIO-66 -NH₂, VAN and AMK, were initially dissolved in DMSO, and then mixed with PBS (Gibco, USA) to a concentration of 0.25 mg/ml. This solution was combined with 10 mg of the synthesized MOFs, and the resulting mixture was stirred for 24 h. Afterward, the mixture was washed three times with ethanol and distilled water, followed by centrifugation at 12,000 rpm for 20 min [27].

The VAN/AMK-UIO-66-NH₂ particles were dispersed evenly in an aqueous solution of PEG (20 mg/mL) using ultrasonication (50 kHz, 100 W L-1) for duration of 5 min in a glass tube with a phenolic cap. Afterwards,

the tube was wrapped in foil to protect it from light and shaken for 24 h. The VAN/AMK-UIO-66-NH₂@PEG particles were separated by centrifugation at 4,000 rpm for 10 min. Following this, the particles were washed three times with deionized water. Finally, the particles were resuspended in deionized water and subjected to freeze-drying for 48 h.

Characterization of VAN/AMK-UIO-66-NH₂@PEG

The morphology of VAN/AMK-UIO-66 -NH₂@PEG was examined by SEM using a TESCAN VEGA 3SB instrument and TEM with a Philips CM30 instrument from the Netherlands. The hydrodynamic diameter and size distribution of the VAN/AMK-UIO-66-NH₂ and VAN/AMK-UIO-66-NH₂@PEG compound were measured using DLS with a Malvern Zetasizer Nano instrument (Malvern Instruments, Worcestershire).

Determination of the entrapment efficiency percent

The entrapment efficiency was assessed by calculating the concentration of VAN and AMK that were not trapped. The complementary medication was extracted from the UIO-66-NH₂ and modified UIO-66-NH₂ solution using Ultracel-30 K Millipore filters with a molecular weight cut-off (MWCO) of 30,000 Da. The formulation was placed in the inner compartment of the cell, with a volume of 500 μL. The setup was then centrifuged for 20 min at 4000×g at 4 °C, using a cooling centrifuge (Eppendorf® 580R centrifuge, Germany). The concentration of free drug in the exterior compartment of the equipment was determined using UV-visible spectrophotometry at 250 and 520 nm (JASCO, V-530, Japan). The EE percent was calculated using Eq. 1 (Eq. 1) [27].

$$\text{Equation 1: EE (\%)} = \frac{\text{Initial drug added} - \text{Free drug}}{\text{Initial drug added}} \times 100$$

In vitro release study of the formulations

The release of VAN and AMK from drugs-loaded UIO-66-NH₂ and UIO-66-NH₂-PEG was investigated using the dialysis diffusion bag method. Accordingly, 2 mL of the MOF suspension was placed into a dialysis bag and sealed.

The dialysis diffusion bag technique was used to evaluate the release of VAN and AMK drug-loaded UIO-66-NH₂ and UIO-66-NH₂@PEG. The molecular weight of the dialysis bag used was 12 kDa (Merck, Germany). Firstly, 2 ml of the MOF suspension was introduced into a dialysis bag and then sealed. The bag was immersed in 50 mL of PBS-SDS (pH 5.4 and 7.4, 37 °C), which served as the medium for releasing or receiving the substance. The bag was then placed on a magnetic stirrer set to 300 RPM. Samples were taken from the buffer compartment at predetermined intervals and replaced with fresh PBS-SDS (Merck, Germany). The OD of each sample was measured at 250 nm and 520 nm. The released VAN

and AMK amounts were estimated using the equation derived from a standard curve. A graph was generated to illustrate the cumulative amount released over time [28].

Determination of the formulations physical stability

The stability of VAN/AMK-UIO-66-NH₂ and VAN/AMK-UIO-66-NH₂@PEG was evaluated for 60 days at two different temperatures (25±2 °C and 4±2 °C). At specific time intervals (14, 30 and 60 days), the structures' dynamic particle size, PDI and EE% were measured and compared to fresh formulations.

Bacterial isolation and characterization

S. aureus isolates were isolated from 500 clinical samples based on their culture characteristics and biochemical tests. The bacteria were isolated from blood, sputum, and urine samples of patients hospitalized at Baqiyatallah Hospital in Tehran between April and September 2023. The biofilm formation ability of the *S. aureus* isolates was evaluated using Congo-red agar and crystal violet assays [28]. Additionally, the presence of the *vanA*, *mecA*, *icaA*, and *icaD* genes in the isolates was assessed using the PCR technique. The antimicrobial sensitivity of the isolates was determined by the Kirby-Bauer disk diffusion susceptibility test. The bacterial isolates that exhibited high biofilm formation potential, show resistance to vancomycin and carried the *vanA* gene (as VRSA isolates) were selected for further investigation.

Antibacterial activity of formulations

The MIC of VAN, AMK, VAN/AMK, VAN/AMK-UIO-66-NH₂, and VAN/AMK-UIO-66-NH₂@PEG was measured using a conventional broth microdilution method with values ranging from 2 to 512 µg/ml. The samples were diluted in a 96-well microplate using Mueller-Hinton broth (MHB). Finally, bacterial suspensions were prepared with a turbidity of 0.5 McFarland by diluting in MHB and added to each well to yield a final concentration of 4–5×10⁵ CFU/ml in wells. The samples were then incubated overnight at 37 °C. The MIC was defined as the lowest concentration at which no bacterial growth was observed. To establish MBC values, 10 µl samples from wells without visible growth were plated on MHA. After overnight incubation, colony counts were used to assess bacterial viability. The MBC was defined as the lowest compound concentration that resulted in the death of 99.9% of the bacterial inoculum [28].

Time-kill assay

The 96-well plate method was applied to conduct time-kill assay. The compounds VAN/AMK, VAN/AMK-UIO-66-NH₂, and VAN/AMK-UIO-66-NH₂@PEG were diluted to concentrations corresponding to their MIC values, following standard procedure. After adding 100 µl

of each sample to a microtiter plate well that had previously been filled with 100 µl of a bacterial solution containing 10⁵ CFU/ml, the plates were incubated at 37 °C. The OD at 600 nm was measured at 8, 16, 24, 32, 40, 48, 56, 64, and 72 h using a microplate reader (EPOCH, Japan). A bacterial growth curve was used as a positive control [29].

Biofilm formation inhibition assay

The ability of the VRSA isolate treated with VAN/AMK, VAN/AMK-UIO-66-NH₂, and VAN/AMK-UIO-66-NH₂@PEG to form biofilm was assessed using a 96-well microtiter plate technique, as previously described [30]. In brief, the isolates were cultured in 96-well microtiter plates for 24 h at 37 °C. The strains were then treated with MIC values of each compound for an additional 24 h at 37 °C. After overnight incubation, the plates were rinsed with PBS to remove non-adherent bacteria. Ultimately, the biofilms were treated with a 1%W/V CV solution and the stain was dissolved in 95% ethanol. The OD of each well was measured at 570 nm using an ELISA reader (Stat Fax 2100, USA). The average absorbance values of each sample were computed and compared to the average values of controls (untreated isolates).

The MBEC was used to assess the ability of the test compounds to disrupt pre-existing biofilms. The strains were allowed to form biofilms as shown in the biofilm formation assessment. Subsequently, the wells were rinsed with sterile PBS, and 200 µL of each tested concentration of VAN/AMK, VAN/AMK-UIO-66-NH₂, and VAN/AMK-UIO-66-NH₂@PEG were added. The plates were incubated for 24 h under aerobic conditions at 37 °C. The OD of the biofilms was then measured at 570 nm. The negative control consisted of uninfected Tryptic Soy broth (Oxoid, USA), whereas the positive control was a simple bacterial culture. The MBEC was defined as the concentration at which the average biofilm OD was equal to or lower than that of negative control. This experiment was conducted in duplicate [31].

Bacterial gene expression in treatment with the formulations

The study aimed to assess the mRNA expression levels of *vanA*, *mecA*, *icaA*, and *icaD* genes in VRSA isolates after being exposed to sub-MIC concentrations of VAN/AMK, VAN/AMK-UIO-66-NH₂, and UIO-66-NH₂@PEG formulations. This was done using qRT-PCR. Firstly, the target genes were identified in VRSA isolates using PCR. The primers used for qRT-PCR are provided in Table 1.

First, total bacterial RNA was extracted following the protocol provided by the RNX-Plus extraction kit (CinnaGen, Iran). Complementary DNA (cDNA) was then synthesized using the RevertAid™ First Strand cDNA

Table 1 Primers used in the current survey

Gene	Primer sequence	Product (bp)
<i>vanA</i>	F: 5'- TCTGCAATAGAGATAGCCGC - 3' R: 3'- GGAGTAGCTATCCCAGCATT - 5'	400
<i>mecA</i>	F: 5'- ATGGTCAAGCCCAGACAGAG-3' R: 3'CGTGTTTTCAACATTTAATGCAA-5'	188
<i>icaA</i>	F: 5'- ATGGTCAAGCCCAGACAGAG - 3' R: 3'- CGTGTTTTCAACATTTAATGCAA - 5'	188
<i>icaD</i>	F: 5'- ATGGTCAAGCCCAGACAGAG - 3' R: 3'- CGTGTTTTCAACATTTAATGCAA - 5'	198
<i>16sRNA</i>	F: 5'- ATCAGAGCGCGGATCTTTGCCG-3' R: 3'- ATCAGAGCGCGGATCTTTGCCG-5'	155

Synthesis Kit, (Fermentas, USA). Afterwards, NanoDrop was used to measure the concentration of the extracted cDNA. The gene expression levels of the examined genes were evaluated via q-RT-PCR using a Master Mix containing SYBER Green (Ampliqon, Denmark). The reactions was conducted in a 25 μ l solution containing 1 μ l of diluted cDNA, one μ l of forward and reverse primers, and 12.5 μ l of SYBR Green Master Mix.

The following steps were used to conduct the qRT-PCR assay: 95 °C for 60 s, 30 cycles of denaturation at 95 °C for 5 s, annealing at 60 °C for 1 min, extension at 72 °C for 45 s, and a final extension at 72 °C for 10 min. The *16 S rRNA* gene was employed as a reference control [32]. The $2^{-\Delta\Delta C_t}$ formula was applied to calculate the fold change in the expression of the target genes, normalized to the reference gene (*16 S rRNA*) and compared to the expression in the untreated sample.

Antioxidant activity

The DPPH test is used to evaluate the antioxidant characteristics of various substances. DPPH is dissolved in ethanol and transformed into its radical form. This radical form exhibits the maximum absorbance level at a wavelength of 517 nm. This radical reacts with antioxidant compounds, leading to its neutralization. As a result, the

absorbance of the solution at 517 nm decreases, causing a color changes from purple to yellow.

This study explores the antioxidant activity of the target compound. To prepare the DPPH radical solution, 1 mg of DPPH was dissolved in 9.16 ml of ethanol. Various concentrations (12.5, 25, 50, 100, 200, and 400 μ g/ml) of VAN/AMK, VAN/AMK-UIO-66-NH₂ and VAN/AMK-UIO-66-NH₂@PEG were prepared and mixed with an equal amount of the DPPH solution. The mixture was vortexed for 10 s and kept in dark environment at room temperature for 30 min. Subsequently, the absorbance of the sample was measured at 517 nm. Butyl hydroxy anisole (BHA) from Merck Germany was utilized as a positive control, while distilled water served as the negative control to compare the effectiveness of the formulations [33].

Statistical analysis

Statistical analysis was conducted using GraphPad Prism (GraphPad Software, San Diego, CA) and SPSS V.20. All tests were performed three times, and the findings were reported as the average values and corresponding standard deviations. The statistical variance analysis technique (ANOVA) was used to assess the differences between the groups. The confidence level was established at 95%, and the results of $p < 0.05$ were considered to have statistical significance.

Results

MOFs characteristics

The morphological analysis using SEM for VAN/AMK-UIO-66@NH₂/PEG showed uniformly distributed particles with a spherical shape and particle size of approximately 200 nm with heterogeneous size distribution (Fig. 1A). TEM imaging of VAN/AMK-UIO-66@NH₂/PEG was utilized, demonstrating a spherical-like structure attributed to the addition of PEG (Fig. 1B). The particle size, PDI, EE% and zeta potential of UIO-66-NH₂,

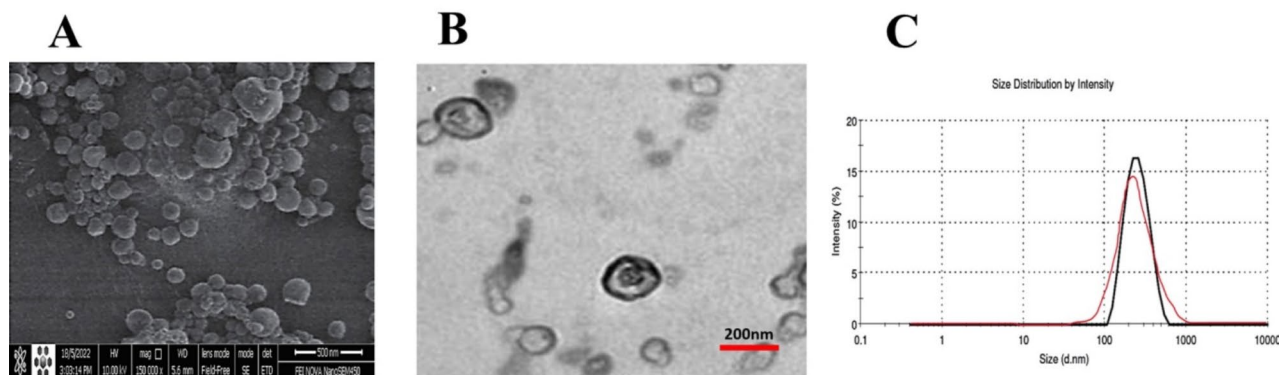


Fig. 1 Morphological and size characterization of VAN/AMK-UIO-66@NH₂/PEG: (A) scanning electron microscopy (SEM), (B) transmission electron microscopy (TEM), and (C) Dynamic Light Scattering (DLS)

VAN/AMK-UIO-66@NH₂ and VAN/AMK-UIO-66@NH₂/PEG are shown in Table 2. The particle size, PDI, and zeta potential of UIO-66@NH₂ were 154.2±2.2 nm, 0.139±0.005 nm and +6.5±1.51 mV, respectively. The average particle size, PDI, EE% and zeta potential of VAN/AMK-UIO-66@NH₂ were 244.3±2.4 nm, 0.166±0.004, 79.2±1.9% (EE for VAN), 76.2±1.9% (EE for AMK) and +7.1±1.98 mV, respectively. The average particle size, PDI, EE% and zeta potential of VAN/AMK-UIO-66@NH₂/PEG were 271.2±2.5 nm, 0.205±0.008, 81.5±3.4% (EE for VAN), 78.95±3.4 (EE for AMK) and +12.4±1.61 mV, respectively. Additionally, the hydrodynamic diameter of VAN/AMK-UIO-66@NH₂ and VAN/AMK-UIO-66@NH₂/PEG nanoparticles which were assessed using the DLS (Zeta sizer), presented in Fig. 1C; Table 2.

Drug release study

This study was carried out to examine the effect of the UIO-66@NH₂ and UIO-66@NH₂/PEG on the release rate of VAN and AMK from the delivery system. Figure 2A and B present the amount of VAN and AMK retained in the different formulations of UIO-66 at specific time intervals, respectively. The results revealed that the release of drugs from UIO-66 formulations followed a biphasic profile, with an initial burst release followed by a sustained or slower release phase.

The amounts of VAN and AMK released from UIO-66@NH₂ and UIO-66@NH₂/PEG were approximately 37.3–44.5% during the first 24 h, indicating the initial phase of release. After this period, the release rate of both drugs remained relatively constant, with a slight change observed for UIO-66@NH₂ and UIO-66@NH₂/PEG in both drugs (48.75% release of VAN and 45.2% release of AMK from PEGylated MOF). There was no significant difference between the release rates of drugs from the UIO-66@NH₂ and UIO-66@NH₂/PEG formulations.

Table 2 The particle size, PDI, EE% and zeta potential of UIO-66-NH₂, VAN/AMK-UIO-66@NH₂ and VAN/AMK-UIO-66@NH₂/PEG

Parameter	UIO-66@NH ₂	VAN/AMK-UIO-66@NH ₂	VAN/AMK-UIO-66@NH ₂ /PEG
Average size (nm)	154.2±2.2	244.3±2.4	271.2±2.5
PDI	0.139±0.005	0.166±0.004	0.205±0.008
Entrapment Efficiency (%) (VAN)	-	79.2±1.9	81.5±3.4
Entrapment Efficiency (%) (AMK)	-	76.2±1.3	78.95±1.8
Zeta potential	+6.5±1.51	+7.1±1.98	+12.4±1.61

Physical stability of MOFs

The physical stability of the VAN/AMK-UIO-66@NH₂ and VAN/AMK-UIO-66@NH₂/PEG formulations was determined by measuring the vesicle size, PDI, EE% and zeta potential in the MOFs before and after two months of storage at two different temperatures (Fig. 3A and B). The samples stored at 4±2 °C were more stable than those stored at 25±2 °C. A significant difference was observed between the stored VAN/AMK-UIO-66@NH₂ and VAN/AMK-UIO-66@NH₂/PEG formulations regarding their particle size and EE% ($P<0.05$). However, no significant difference was found in their PDI and zeta potential. In both formulations, the PDI of the nanoparticles changed after 30 days of storage at 25±2 °C and after 60 days at both temperatures ($P<0.01$). Changes in zeta potential of both formulations were only significant after 60 days of storage at 25±2 °C ($P<0.05$). The inclusion of PEG in the formulation exhibited a preserving effect on the EE% and particle size after 30 and 60 days of storage, respectively.

VRSA identification and biofilm formation ability

Among 500 clinical isolates, we identified 128 isolates as *S. aureus* strains using biochemical tests, including Gram staining, catalase, oxidase, coagulase, etc. Among 128 *S. aureus* isolates, we further identified 13 VRSA isolates. These isolates exhibited high-level vancomycin (MIC≥64 µg/ml). Based on their resistance to glycopeptide and beta-lactam antibiotics, the VRSA isolates expressed *vanA* and *mecA* phenotypes, which were confirmed using conventional PCR.

According to the CV test, All 13 VRSA isolates formed biofilms to various degrees; 10 isolates formed strong biofilms (OD≥0.49±0.005), and 3 produced moderate biofilms (Table 3). The PCR technique also revealed that the strong biofilm producers carried *icaA* and *icaD* genes in their genomes.

Antibacterial activity of the prepared formulations

The MICs and MBCs of VAN, AMK, VAN/AMK, VAN/AMK-UIO-66@NH₂, and VAN/AMK-UIO-66@NH₂/PEG against *S. aureus* ATCC 29,213 and 10 clinical isolates of VRSA were presented in Tables 4 and 5, respectively. The MIC values of VAN, AMK, VAN/AMK, VAN/AMK-UIO-66@NH₂, and VAN/AMK-UIO-66@NH₂/PEG against strong biofilm-producers (clinical isolates) were ≥64 µg/ml, ≥128 µg/ml, ≥16 µg/ml, ≥4 µg/ml and ≥2 µg/ml, respectively. The MBC values of VAN, AMK, VAN/AMK, VAN/AMK-UIO-66@NH₂, and VAN/AMK-UIO-66@NH₂/PEG against selected isolates were also ≥128 µg/ml, ≥256 µg/ml, ≥32 µg/ml, ≥8 µg/ml and ≥4 µg/ml, respectively. These results demonstrate that the MICs and MBCs of VAN/AMK-UIO-66@NH₂/PEG were significantly lower ($P<0.05$) compared to

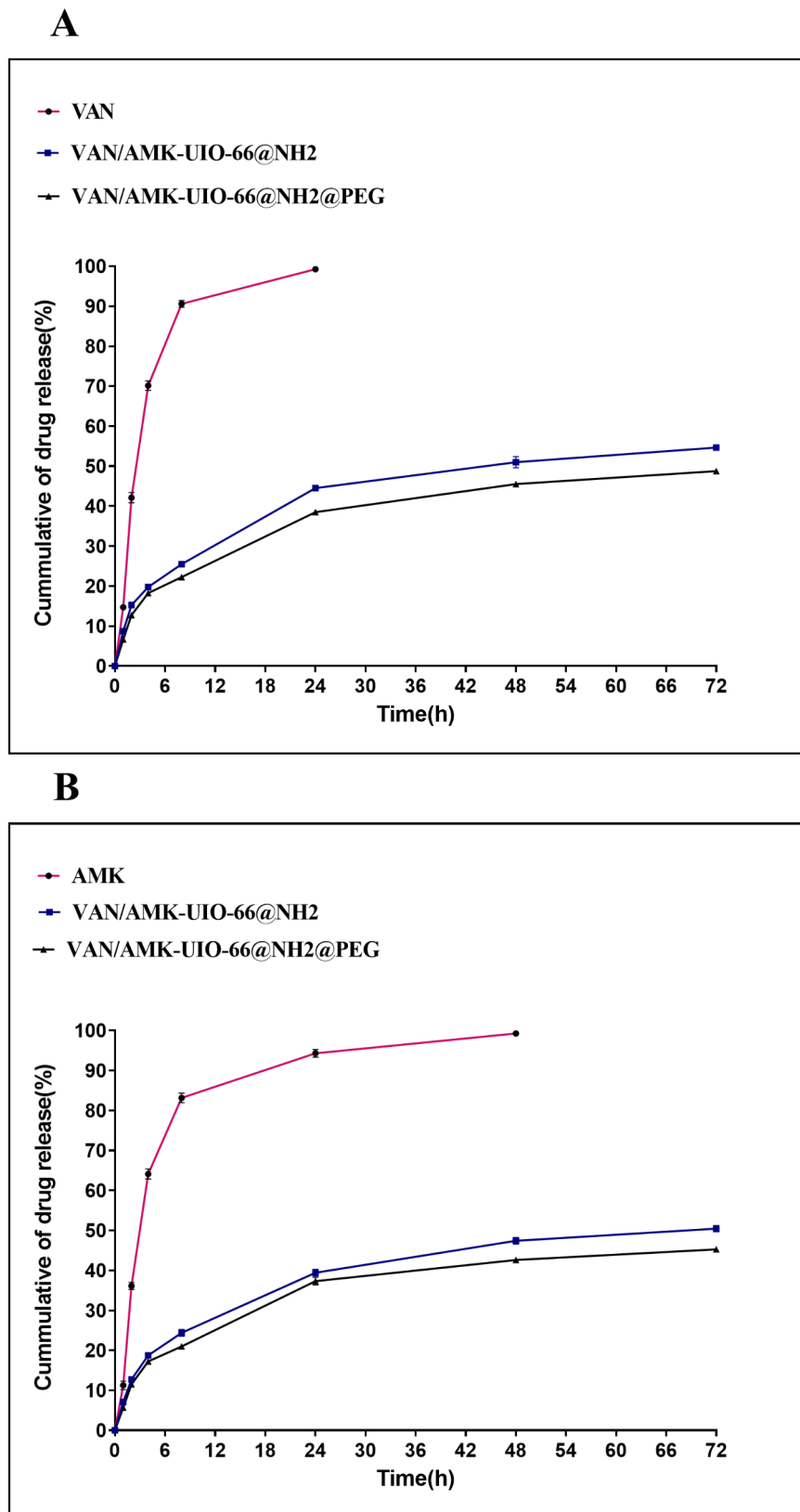


Fig. 2 In vitro drug release profile of accessible VAN (A) and AMK (B) in UIO-66@NH₂ and UIO-66@NH₂/PEG. Data are represented as mean ± SD

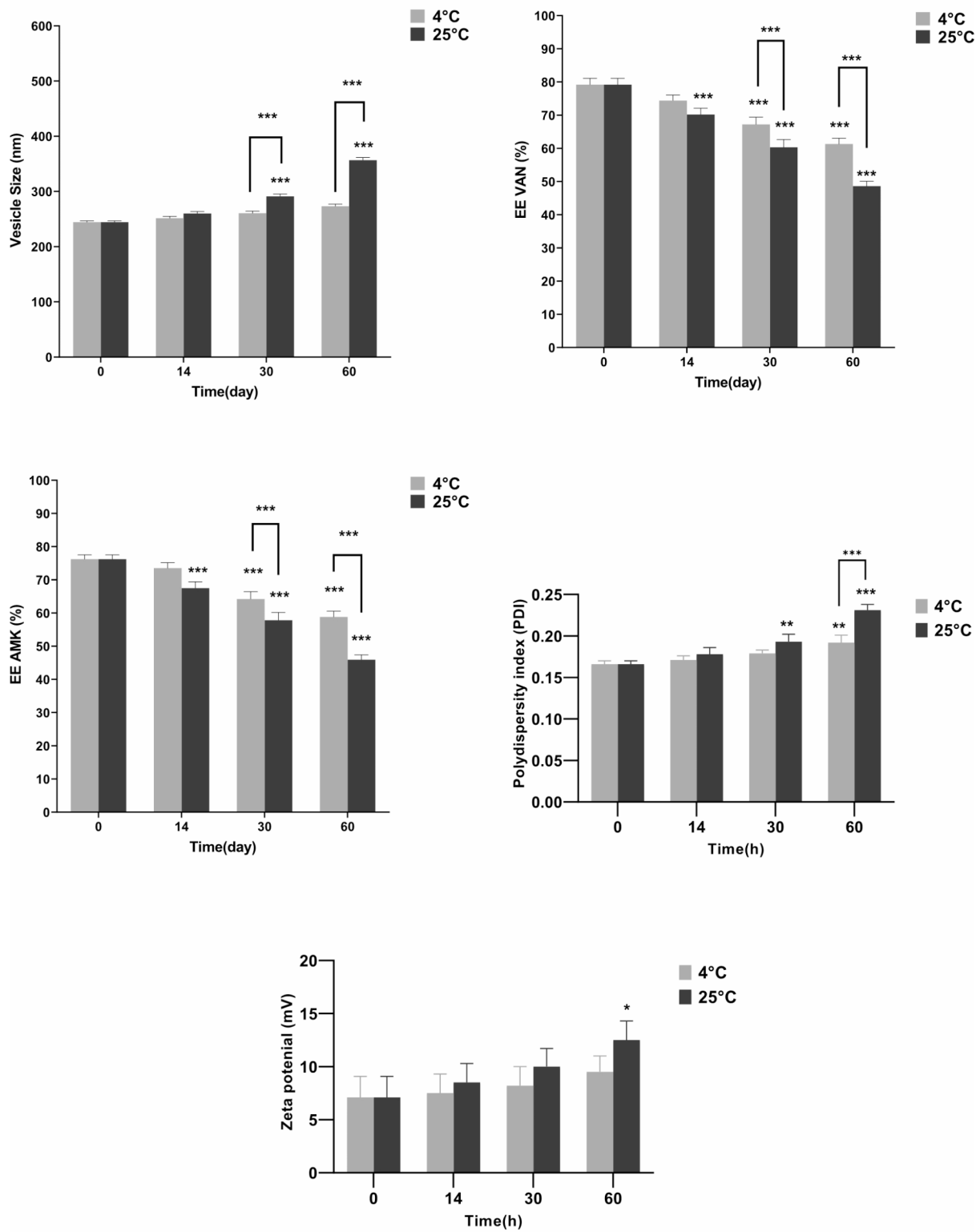


Fig. 3 The physical stability of the (A) VAN/AMK-UIO-66@NH₂ and (B) VAN/AMK-UIO-66@NH₂/PEG formulations was determined by measuring the vesicle size, PDI, EE VAN%, EE AMK% and zeta potential in the MOFs before and after two months of storage at 4 ± 2 °C and 4 ± 2 °C. Data are represented as mean ± SD. (*: *p* < 0.05, **: *p* < 0.01 and ***: *p* < 0.001)

Table 3 Biofilm formation ability of 13 VRSA isolates

Strain NO.	Strong biofilm	Medium biofilm	Weak biofilm
1	0.62 ± 0.006	-	-
2	0.6 ± 0.003	-	-
3	0.55 ± 0.005	-	-
4	0.58 ± 0.005	-	-
5	0.51 ± 0.005	-	-
6	-	0.41 ± 0.005	-
7	0.53 ± 0.003	-	-
8	0.565 ± 0.004	-	-
9	-	0.43 ± 0.004	-
10	-	0.38 ± 0.006	-
11	0.49 ± 0.005	-	-
12	0.53 ± 0.003	-	-
13	0.59 ± 0.006	-	-
ATCC 29,213	-	0.45 ± 0.003	-

treatments with VAN, AMK, VAN/AMK, VAN/AMK-UIO-66@NH₂.

Time kill assay

The antimicrobial activity of VAN/AMK, VAN/AMK-UIO-66@NH₂, and VAN/AMK-UIO-66@NH₂/PEG against ten biofilm-producing clinical isolates of VRSA was investigated using a time-kill assay. As shown in Fig. 4A, VAN/AMK-UIO-66@NH₂/PEG at MIC concentrations demonstrated enhanced killing of VRSA isolates compared VAN/AMK and VAN/AMK-UIO-66@NH₂ after 72 h. Notably, the MIC concentration of VAN/AMK-UIO-66@NH₂ increased the killing effect by approximately twice as much as the combined drugs alone. The combination of VAN/AMK-UIO-66@NH₂/PEG exhibited sustained and potent lethality against VRSA clinical isolates up to 32 h, after which bacterial growth gradually slowed down.

Anti-biofilm activity of the prepared formulations

The VAN/AMK, VAN/AMK-UIO-66@NH₂, and VAN/AMK-UIO-66@NH₂/PEG were evaluated for their ability

Table 4 MICs of VAN, AMK, VAN/AMK, VAN/AMK-UIO-66@NH₂, and VAN/AMK-UIO-66@NH₂/PEG against laboratory *S. aureus* strain ATCC 29,213 and 10 clinical isolates of VRSA

Strain No.	MIC-VAN (µg/ml)	MIC-AMK (µg/ml)	MIC-VAN/AMK	MIC-VAN/AMK-UIO-66-NH ₂ (µg/ml)	MIC-VAN/AMK-UIO-66-NH ₂ @PEG (µg/ml)
1	128	256	32	8	4
2	128	256	32	8	8
3	64	128	16	4	2
4	128	128	32	8	4
5	64	128	16	4	2
7	64	128	16	4	4
8	64	128	16	4	2
11	64	256	32	8	4
12	64	128	16	4	2
13	128	256	32	8	4
ATCC 29,213	64	64	16	4	2

Table 5 MBCs of VAN, AMK, VAN/AMK, VAN/AMK-UIO-66@NH₂, and VAN/AMK-UIO-66@NH₂/PEG against laboratory *S. aureus* strain ATCC 29,213 and 10 clinical isolates of VRSA

Strain NO.	MBC-VAN (µg/ml)	MBC-AMK (µg/ml)	MBC-VAN/AMK	MBC-VAN/AMK-UIO-66-NH ₂ (µg/ml)	MBC-VAN/AMK-UIO-66-NH ₂ @PEG (µg/ml)
1	256	512	64	16	8
2	256	512	64	16	16
3	128	256	32	8	4
4	256	256	64	16	8
5	128	256	32	8	4
7	128	256	32	8	8
8	128	256	32	8	4
11	128	512	64	16	8
12	128	256	32	8	4
13	256	512	64	16	8
ATCC 29,213	128	128	32	8	4

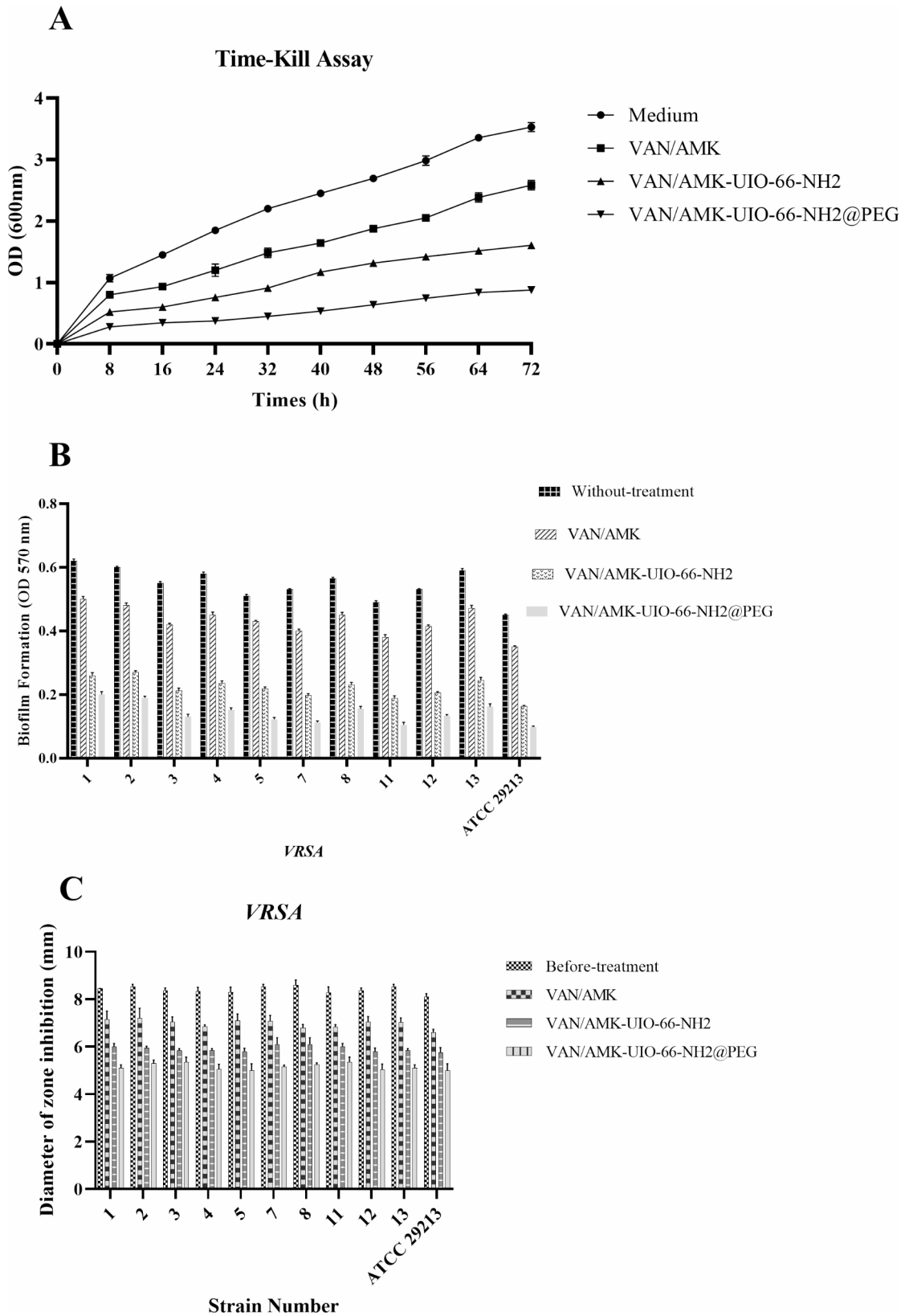


Fig. 4 The (A) Time-Kill assay and (B) CV test and (C) MBEC test of VAN/AMK, VAN/AMK-UIO-66@NH₂, and VAN/AMK-UIO-66@NH₂/PEG against ten biofilm-producing clinical isolates of VRSA. Data are represented as mean ± SD

to inhibit biofilm formation by *S. aureus* ATCC 29,213 and 10 biofilm-producing clinical isolates of VRSA. As shown in Fig. 4B, all three formulations inhibited biofilm formation at sub-MIC concentrations. VAN/AMK-UIO-66@NH₂/PEG was found to inhibit biofilm formation at sub-MIC (1 µg/ml) as compared to the untreated biofilm control, and VAN/AMK (more than 3.5-folds), VAN/AMK-UIO-66@NH₂ (approximately 2-folds in some cases) treatments ($P < 0.001$). Figure 4C also indicated that VAN/AMK, VAN/AMK-UIO-66@NH₂, and VAN/AMK-UIO-66@NH₂/PEG formulations can significantly reduce MBEC value compared to control ($p < 0.001$). However, VAN/AMK-UIO-66@NH₂/PEG exhibited the most reduction in the MBEC value, which confirms its great anti-biofilm activity.

Bacterial gene expression in treatment with the formulations

To investigate the potential interaction between VAN/AMK-UIO-66@NH₂/PEG and resistant as well as biofilm-related genes, VRSA isolates treated with VAN/AMK, VAN/AMK-UIO-66@NH₂, and VAN/AMK-UIO-66@NH₂/PEG. The transcription level of *mecA*, *vanA*, *icaA*, and *icaD* genes were analyzed using qRT-PCR. Our finding revealed a significant downregulation ($p < 0.001$) in the expression of these genes in isolates treated with VAN/AMK-UIO-66@NH₂ and VAN/AMK-UIO-66@NH₂/PEG compared to the control and VAN/AMK treatments. Notably, the VAN/AMK-UIO-66@NH₂/PEG formulation exhibited the superior efficacy compared to the other formulations (Fig. 5). This suggests that the pegylated MOF loaded with dual drugs exhibits significant anti-biofilm and anti-quorum sensing properties.

Antioxidant activity

The DPPH assay was used to evaluate the radical scavenging activity of VAN/AMK, VAN/AMK-UIO-66@NH₂, and VAN/AMK-UIO-66@NH₂/PEG. As shown in Fig. 6, the radical scavenging activity of activity of both VAN/AMK-UIO-66@NH₂ and VAN/AMK-UIO-66@NH₂/PEG at various concentrations was significantly higher than that of VAN/AMK ($P < 0.001$). Furthermore, VAN/AMK-UIO-66@NH₂/PEG exhibited a considerably greater radical scavenging activity compared to VAN/AMK-UIO-66@NH₂ with a statistically significant difference across the tested concentrations ($p < 0.001$). At a concentration of 400 µg/mL, VAN/AMK-UIO-66@NH₂/PEG exhibited the highest radical scavenging activity, achieving an impressive 74.33% inhibition of DPPH free radicals.

Discussion

S. aureus, specifically MRSA and VRSA, is a highly concerning bacterial species that is becoming increasingly resistant to multiple drugs worldwide [34]. This bacterium is a dangerous pathogen that can cause severe medical conditions in both community and settings [35]. These conditions include pneumonia, skin infections, joint inflammation, heart valve infections, and mastitis. The emergence of VRSA has further exacerbated this issue [36]. VRSA's ability to resist the effects of antimicrobial drugs and evade the host immune response is driven by antimicrobial resistance and the presence of virulence-related genes. The increased severity of VRSA infections may be attributed to its production of several toxins and its ability to develop biofilms. These factors enable the germs to survive and become more resistant while evading the immune system [37].

The lack of new antibiotic development, coupled with the rise of microbial resistance, is likely to increase morbidity and mortality, particularly in hospitals. Therefore new strategies are urgently needed to prevent and eliminate bacterial biofilm to improve current treatment approaches [38]. The present study thoroughly evaluated the use of drug-loaded vehicles to control bacterial biofilms. MOFs play a crucial role as antibacterial agents for such applications. Antimicrobial materials based on MOFs have several unique properties: (i) MOFs possess a high specific surface area and porosity, enabling them to be loaded with metal ions or antibacterial drugs with bactericidal properties. These agents can be released gradually in response to stimuli like pH changes or laser irradiation [39]. (ii) The flexibility in using a range various metals and linkers allows the creation of highly biocompatible MOFs by choosing non-toxic or less-toxicity precursors [40]. (iii) MOFs possess several surface-active groups that enable easy modification, allowing them to target specific bacterial infection sites and facilitating the release of antibacterial drugs [40]. Compared to other antibacterial nanomaterials, MOFs offer distinct advantages. Their porous structure allows for efficient encapsulation of antibacterial agents such as metal/metal oxide nanoparticles, antibiotics, antibacterial peptides, and natural antibacterial substances. The responsive degradable framework ensures controlled or gradual release of metal ions, organic ligands, and antibacterial agents as needed. Additionally, their ability to be easily modified enhances their compatibility with living organisms [41].

The ability of VRSA to form biofilms is a key factor in its pathogenicity, enabling it to resist antibiotics and elude the host's defensive. Biofilms are aggregations of bacteria or other microorganisms that adhere to surfaces and form a protective framework of extracellular polymeric substances (EPS) [42]. Biofilms are highly resistant to antibiotics and the host immune response,

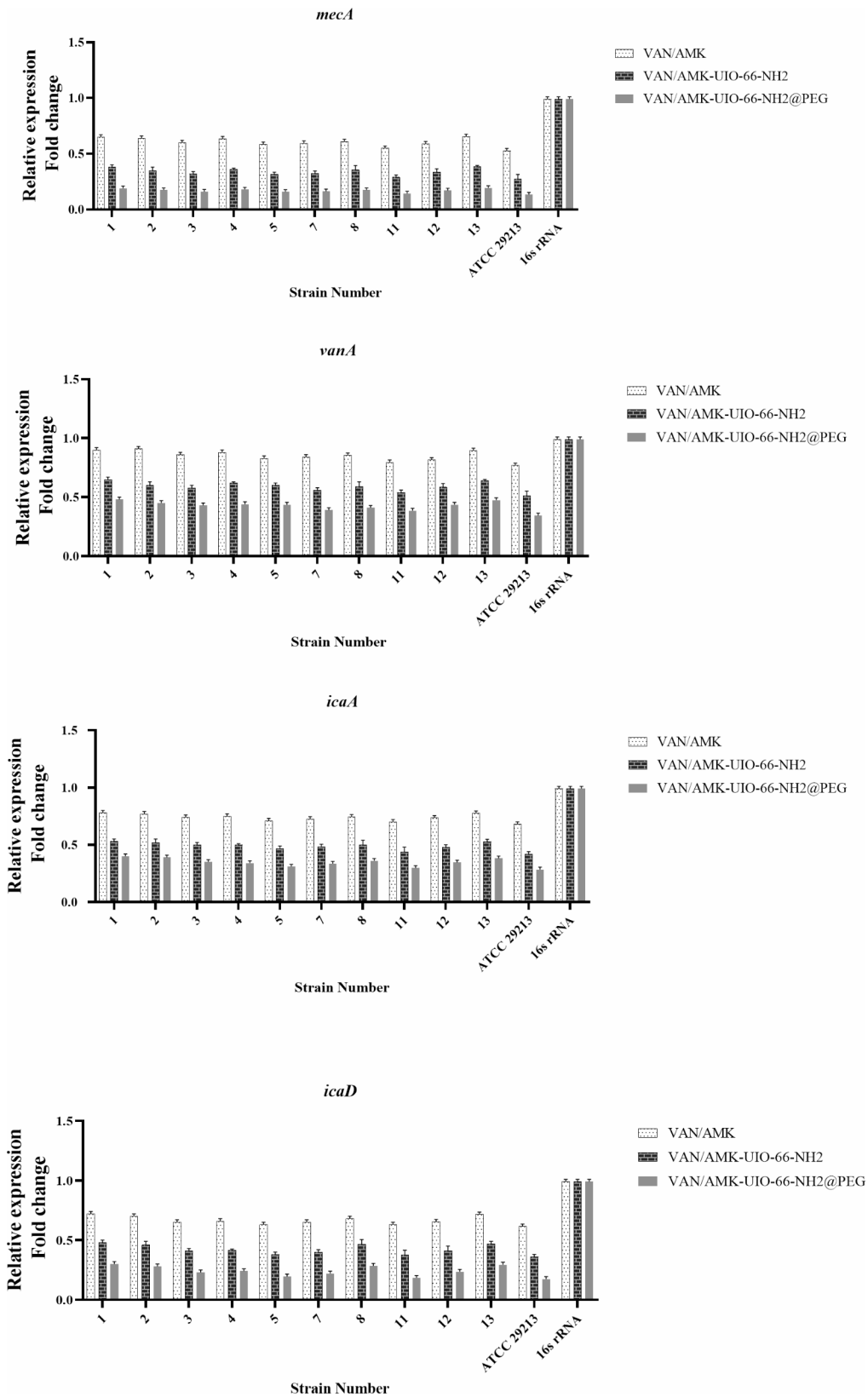


Fig. 5 VAN/AMK, VAN/AMK-UIO-66@NH₂, and VAN/AMK-UIO-66@NH₂/PEG effects on the alteration of *mecA*, *vanA*, *icaA* and *icaD* genes expression in VRSA isolates. Data are represented as mean ± SD

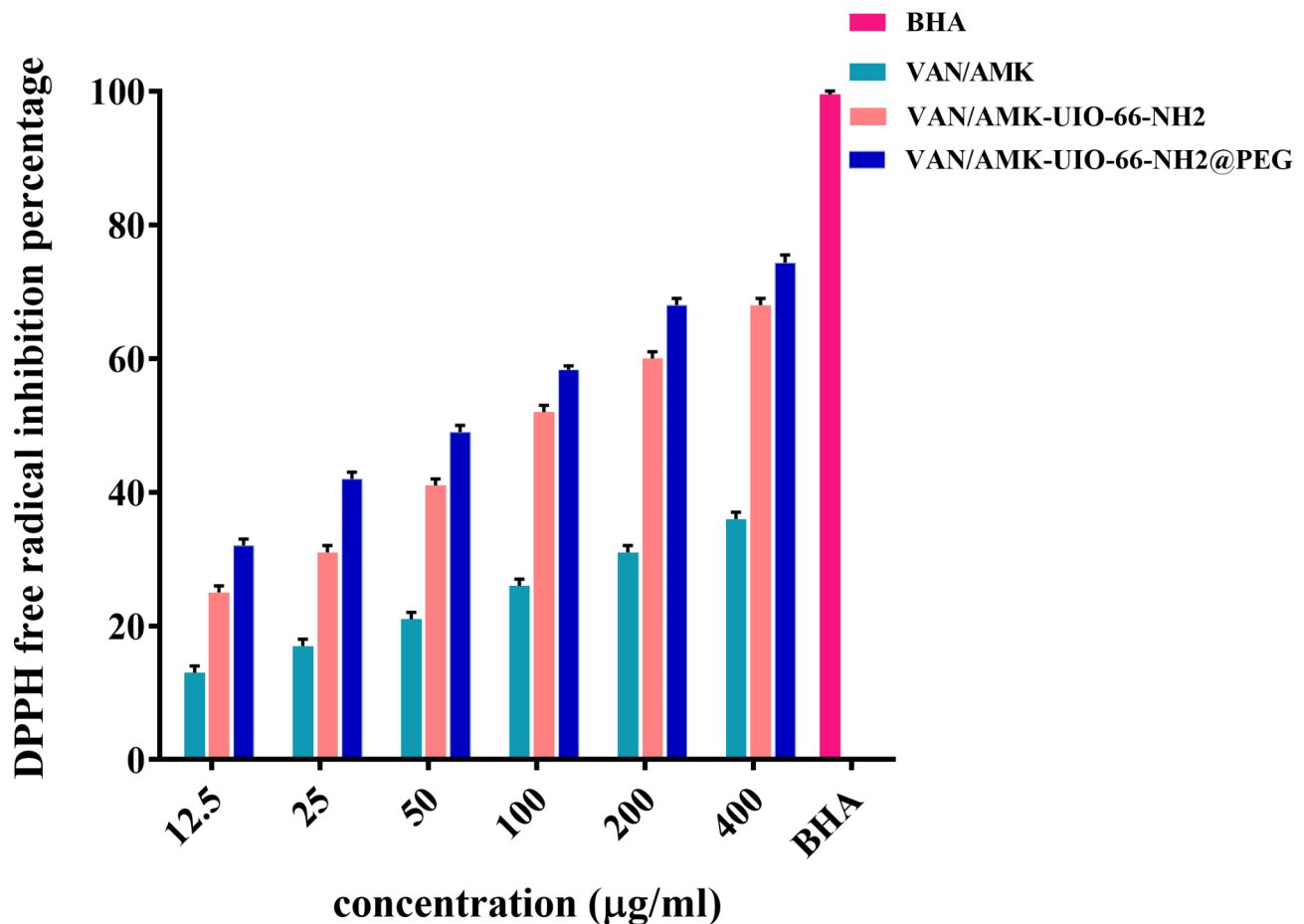


Fig. 6 The radical scavenging activity of VAN/AMK, VAN/AMK-UIO-66@NH₂, and VAN/AMK-UIO-66@NH₂/PEG compared to BHA using DPPH methods. Data are represented as mean ± SD

making them a significant in medical, industrial, and environmental contexts. Several comprehensive study have shown that various MOFs f have antibacterial, anti-biofilm, and antioxidant properties. MOFs can prevent biofilm formation by either killing bacteria or interfering with their quorum sensing, the communication system that regulate their collective behavior [43]. Some examples of MOFs that have antibacterial and anti-biofilm properties are NH₂-MIL-125, ZIF, and Ni-MOF [34, 44, 45].

Here, among 128 *S. aureus* clinical isolates, we identified 13 VRSA isolates. These isolates showed high-level vancomycin resistance (MIC ≥ 64 µg/ml). Based on their resistance to glycopeptide and beta-lactam antibiotics, the VRSA isolates expressed *vanA* and *mecA* phenotypes, which were identified using conventional PCR. Of the 13 VRSA isolates, 10 were capable of forming robust biofilms, containing both the *icaA* and *icaD* genes. The antibacterial study demonstrated that, in contrast to the free drugs, the VAN/AMK-UIO-66@NH₂/PEG formulation exhibited significantly enhanced antibacterial potency against the VRSA isolates. The MIC of VAN/

AMK-UIO-66@NH₂/PEG was extremely 32-fold lower than VAN, 64-fold lower than AMK, 8-fold lower than VAN/AMK and 2-fold lower than VAN/AMK-UIO-66@NH₂. This indicates that a lower concentration of VAN/AMK-UIO-66@NH₂/PEG is required to inhibit microbial growth compared to the VAN, AMK, VAN/AMK, and VAN/AMK-UIO-66@NH₂. Time-kill study indicated that VAN/AMK-UIO-66@NH₂/PEG showed the highest sensitivity and most significant reduction in VRSA isolate growth, consistent with the MIC results. Furthermore, the greater penetration of VAN/AMK-UIO-66@NH₂/PEG into bacterial cells and its improved drug release allowed for more effective bacterial killing and significant reduction in biofilm formation compared to VAN/AMK and VAN/AMK-UIO-66@NH₂. Functionalized and modified MOFs may act as drug delivery systems within the biofilm matrix, as biofilms play a significant role in antibiotic resistance [46]. To confirm the phenotyping characterization of the anti-biofilm activity of the formulations, we conducted a molecular study of resistant- and biofilm-associated genes. The results showed that the transcription level of the *mecA*, *vanA*, *icaA*, and

icaD genes in VAN/AMK-UIO-66@NH₂/PEG treated with VAN/AMK-UIO-66@NH₂/PEG were significantly lower than in those treated with VAN/AMK or VAN/AMK-UIO-66@NH₂. This indicates that VAN/AMK-UIO-66@NH₂/PEG has anti-biofilm and anti-quorum sensing properties. The reduction in gene expression in biofilm formation and quorum sensing may be attributed to direct interactions between VAN/AMK and transcription factors involved in biofilm regulation. Our findings are consistent with research conducted by Zhou et al., which showed that UIO-66 loaded with caffeic acid could disrupt the surface morphology and ultrastructure of *E. coli* and *S. aureus*. The MBC for *E. coli* and *S. aureus* was 1.0 mg/mL and 2.0 mg/mL, respectively [47]. In another study, the antibacterial activity of ciprofloxacin, UIO-66, and CIP-UIO-66 against *S. aureus* and *E. coli* was evaluated using the disk diffusion method and CIP-UIO-66 exhibited the largest inhibition zone against both bacteria, attributed to its regulated release mechanism [32]. Additionally, Karakeçili study revealed that fosfomicin-loaded UIO-66 nanocrystals incorporated into wet-spun chitosan scaffolds had bactericidal effects against *S. aureus* [48]. In another study, time-kill assay showed that Ag/UIO-66-NH₂ exhibited the most potent inhibitory effect against both *S. aureus* and *E. coli* strains at higher concentrations [49]. The synergistic antibacterial action of UIO-66@NH₂-PEG may be explained by its ability to penetrate and disrupt bacterial cell walls, facilitating the entry of VAN and AMK and enhancing their bactericidal effects [50].

In addition to antibacterial activity, the antioxidant properties of the samples were assessed. The results demonstrated that the radical scavenging activity of VAN/AMK-UIO-66@NH₂/PEG was substantially higher than that of VAN/AMK-UIO-66@NH₂ or other formulations at various concentrations. This suggests that the antioxidant activity of drugs encapsulated in UIO-66@NH₂/PEG was greatly improved at lower doses. The notable antioxidant properties of VAN/AMK-UIO-66@NH₂/PEG may be attributed to its enhanced solubility and superior ability to adsorb DPPH radicals.

Conclusion

In the present study, VAN and AMK were successfully loaded into UIO-66-NH₂@PEG metal-organic frameworks and characterized in terms of particle size, PDI, EE%, zeta potential, controlled release and physical stability. Our finding demonstrated that VAN/AMK-UIO-66@NH₂/PEG exhibited significantly higher antibacterial and anti-biofilm activities against VRSA strains compared to VAN, AMK, VAN/AMK, and VAN/AMK-UIO-66@NH₂ formulations. These findings underscore the efficacy of VAN/AMK-UIO-66@NH₂/PEG in disrupting resistance mechanisms and biofilm formation by showcasing

its antioxidant properties and downregulating of resistance- and biofilm-associated genes. Further researches are needed to investigate the underlying mechanisms of VAN/AMK-UIO-66@NH₂/PEG's effects on MDR bacteria. Moreover, extensive studies are recommended to assess the impact of this formulation on human tissues and cells, to determine its potential toxicity in human applications.

Acknowledgements

The data presented in this study are available from the corresponding author (S.A) upon request.

Author contributions

N.R, P.M and F.A performed the laboratory experiments. S.A wrote the manuscript. A.S prepared figures and edited the manuscript. All authors reviewed and confirm the manuscript.

Funding

This work was supported by the Islamic Azad University.

Data availability

Data is provided within the manuscript or supplementary information files.

Declarations

Ethics approval and consent to participate

The present study was approved by the Institutional Review Board (IRB) of the Islamic Azad University, Tehran, Iran, under the ethical code 9/9/300819. For any aspects of the study that involved human subjects, written informed consent was obtained from all participants or their legal guardians, as applicable.

Consent for publication

Not applicable.

Competing interests

The authors declare no competing interests.

Conflict of interest

The authors declare that there are no conflicts of interest.

Author details

¹Faculty of Pharmacy, Tehran Medical Sciences, Islamic Azad University, Tehran, Iran

²Department of Biology, North Tehran Branch, Islamic Azad University, Tehran, Iran

³Department of Animal Science, Faculty of Agriculture, University of Kurdistan, Sanandaj, Kurdistan, Iran

⁴Department of Microbiology and Immunology, Faculty of Veterinary Medicine, University of Tehran, Tehran, Iran

Received: 26 July 2024 / Accepted: 29 October 2024

Published online: 08 November 2024

References

1. Yoshikawa TT, Bradley SF. *S. aureus* infections and antibiotic resistance in older adults. *Clin Infect Dis*. 2002;34(2):211–6.
2. Tong SY, Davis JS, Eichenberger E, Holland TL, Fowler VG Jr. *Aureus* infections: epidemiology, pathophysiology, clinical manifestations, and management. *Clin Microbiol Rev*. 2015;28(3):603–61.
3. Chambers HF, DeLeo FR. Waves of resistance: *S. Aureus* in the antibiotic era. *Nat Rev Microbiol*. 2009;7(9):629–41.
4. Sharifi A, Sobhani K, Mahmoudi P. A systematic review and meta-analysis revealed a high-level antibiotic resistance of bovine mastitis *Staphylococcus aureus* in Iran. *Res Vet Sci*. 2023;161:23–30.

5. Mlynarczyk-Bonikowska B, Kowalewski C, Krolak-Ulinska A, Marusza W. Molecular mechanisms of drug resistance in *S. Aureus*. *Int J Mol Sci*. 2022;23(15):8088.
6. Shore A, Rossney AS, Keane CT, Enright MC, Coleman DC. Seven novel variants of the staphylococcal chromosomal cassette mec in methicillin-resistant *S. Aureus* isolates from Ireland. *Antimicrob Agents Chemother*. 2005;49(5):2070–83.
7. Cong Y, Yang S, Rao X. Vancomycin resistant *S. aureus* infections: a review of case updating and clinical features. *J Adv Res*. 2020;21:169–76.
8. Hiramatsu K. Vancomycin-resistant *S. aureus*: a new model of antibiotic resistance. *Lancet Infect Dis*. 2001;1(3):147–55.
9. Arthur M, Molinas C, Depardieu F, Courvalin P. Characterization of Tn1546, a Tn3-related transposon conferring glycopeptide resistance by synthesis of depsipeptide peptidoglycan precursors in *Enterococcus faecium* BM4147. *J Bacteriol*. 1993;175(1):117–27.
10. White BP, Lomaestro B, Pai MP. Optimizing the initial amikacin dosage in adults. *Antimicrob Agents Chemother*. 2015;59(11):7094–6.
11. Pacifici GM, Marchini G. Clinical pharmacokinetics of amikacin in neonates. *Int J Pediatr*. 2017;5(2):4407–28.
12. Chow VC, Hawkey PM, Chan EW, Chin ML, Au T, Fung DK, Chan RC. High-level gentamicin resistance mediated by a tn 4001-like transposon in seven nonclonal hospital isolates of *Streptococcus pasteurianus*. *Antimicrob Agents Chemother*. 2007;51(7):2508–13.
13. Ramirez MS, Tolmasky ME. Amikacin: uses, resistance, and prospects for inhibition. *Molecules*. 2017;22(12):2267.
14. Karygianni L, Ren Z, Koo H, Thurnheer T. Biofilm matrixome: extracellular components in structured microbial communities. *Trends Microbiol*. 2020;28(8):668–81.
15. Guo H, Tong Y, Cheng J, Abbas Z, Li Z, Wang J, et al. Biofilm and small colony variants—an update on *S. aureus* strategies toward drug resistance. *Int J Mol Sci*. 2022;23(3):1241.
16. Cramton SE, Gerke C, Schnell NF, Nichols WW, Götz F. The intercellular adhesion (ica) locus is present in *S. Aureus* and is required for biofilm formation. *Infect Immun*. 1999;67(10):5427–33.
17. O’Gara JP. ica and beyond: biofilm mechanisms and regulation in *Staphylococcus epidermidis* and *S. aureus*. *FEMS Microbiology Letters*. 2007;270(2):179–88.
18. Gerke C, Kraft A, Sußmuth R, Schweitzer O, Götz F. Characterization of then-acetylglucosaminyltransferase activity involved in the biosynthesis of the *Staphylococcus epidermidis* Polysaccharide Intercellular Adhesin. *J Biol Chem*. 1998;273(29):18586–93.
19. Umemura A, Diring S, Furukawa S, Uehara H, Tsuruoka T, Kitagawa S. Morphology design of porous coordination polymer crystals by coordination modulation. *J Am Chem Soc*. 2011;133(39):15506–13.
20. Wyszogrodzka G, Marszałek B, Gil B, Dorożyński P. Metal-organic frameworks: mechanisms of antibacterial action and potential applications. *Drug Discovery Today*. 2016;21(6):1009–18.
21. Abánades Lázaro I, Wells CJ, Forgan RS. Multivariate Modulation of the zr MOF UiO-66 for defect-controlled combination Anticancer Drug Delivery. *Angew Chem*. 2020;132(13):5249–55.
22. Zhu X, Gu J, Wang Y, Li B, Li Y, Zhao W, Shi J. Inherent anchorages in UiO-66 nanoparticles for efficient capture of alendronate and its mediated release. *Chem Commun*. 2014;50(63):8779–82.
23. Cunha D, Gaudin C, Colinet I, Horcajada P, Maurin G, Serre C. Rationalization of the entrapment of bioactive molecules into a series of functionalized porous zirconium terephthalate MOFs. *J Mater Chem B*. 2013;1(8):1101–8.
24. Yan B, Tan J, Zhang H, Liu L, Chen L, Qiao Y, Liu X. Constructing fluorine-doped Zr-MOF films on titanium for antibacteria, anti-inflammation, and osteogenesis. *Biomaterials Adv*. 2022;134:112699.
25. Alavi SE, Cabot PJ, Moyle PM. Glucagon-like peptide-1 receptor agonists and strategies to improve their efficiency. *Mol Pharm*. 2019;16(6):2278–95.
26. Kenechukwu FC, Nnamani DO, Momoh MA, Attama AA. Enhanced circulation longevity and pharmacodynamics of metformin from surface-modified nanostructured lipid carriers based on solidified reverse micellar solutions. *Heliyon*. 2022;8(3).
27. Bazzazan S, Moeinabadi-Bidgoli K, Lalami ZA, Bazzazan S, Mehrarya M, Yeganeh FE, et al. Engineered UiO-66 metal-organic framework for delivery of curcumin against breast cancer cells: an in vitro evaluation. *J Drug Deliv Sci Technol*. 2023;79:104009.
28. Shiri M, Ashrafi F. The bactericidal and Antibiofilm effects of New liposomes Containing Vancomycin Formulation against clinical biofilm positive *S. Aureus* isolates. *Appl Biochem Microbiol*. 2023;59(6):824–32.
29. Sadeghi S, Bakhshandeh H, Ahangari Cohan R, Peirovi A, Ehsani P, Norouzi D. Synergistic anti-staphylococcal activity of niosomal recombinant lysostaphin-LL-37. *Int J Nanomed*. 2019:9777–92.
30. Dastneshan A, Rahiminezhad S, Mezajin MN, Jevinani HN, Akbarzadeh I, Abdihaji M, et al. Cefazolin encapsulated UiO-66-NH2 nanoparticles enhance the antibacterial activity and biofilm inhibition against drug-resistant *S. aureus*: in vitro and in vivo studies. *Chem Eng J*. 2023;455:140544.
31. Barakat HS, Kassem MA, El-Khordagui LK, Khalafallah NM. Vancomycin-eluting niosomes: a new approach to the inhibition of staphylococcal biofilm on abiotic surfaces. *AAPS PharmSciTech*. 2014;15:1263–74.
32. Weinstein MP, Lewis JS 2. nd. The Clinical and Laboratory Standards Institute Subcommittee on Antimicrobial susceptibility testing: background, Organization, functions, and processes. *J Clin Microbiol*. 2020;58(3).
33. Shin SW, Song IH, Um SH. Role of physicochemical properties in nanoparticle toxicity. *Nanomaterials*. 2015;5(3):1351–65.
34. Ammar A, Abd El-Hamid MI, Eid SE, El Oksh AS. Insights into antimicrobial resistance and virulence genes of emergent multidrug resistant avian pathogenic *Escherichia coli* in Egypt: how closely related are they. *Rev Med Vet*. 2015;166(9–10):304–14.
35. Elmowalid GAE, Ahmad AAM, El-Hamid MIA, Ibrahim D, Wahdan A, El Oksh AS, et al. Nigella sativa extract potentially inhibited methicillin resistant *S. aureus* induced infection in rabbits: potential immunomodulatory and growth promoting properties. *Animals*. 2022;12(19):2635.
36. Dhanalakshmi T, Umapathy B, Mohan D. Prevalence of Methicillin, Vancomycin and Multidrug Resistance among *S. Aureus*. *J Clin Diagn Res*. 2012;6(6).
37. Abd El-Hamid MI, Ibrahim D, Elazab ST, Gad WM, Shalaby M, El-Neshwy WM, et al. Tackling strong biofilm and multi-virulent Vancomycin-resistant *S. Aureus* via natural alkaloid-based porous nanoparticles: perspective towards near future eradication. *Front Cell Infect Microbiol*. 2024;13:1287426.
38. Abdelghafar A, Yousef N, Askoura M. Zinc oxide nanoparticles reduce biofilm formation, synergize antibiotics action and attenuate *S. Aureus* virulence in host; an important message to clinicians. *BMC Microbiol*. 2022;22(1):244.
39. Wang Y, Yan J, Wen N, Xiong H, Cai S, He Q, et al. Metal-organic frameworks for stimuli-responsive drug delivery. *Biomaterials*. 2020;230:119619.
40. Ma Y, Qu X, Liu C, Xu Q, Tu K. Metal-organic frameworks and their composites towards biomedical applications. *Front Mol Biosci*. 2021;8:805228.
41. Guo L, Kong W, Che Y, Liu C, Zhang S, Liu H, et al. Research progress on antibacterial applications of metal-organic frameworks and their biomacromolecule composites. *Int J Biol Macromol*. 2024;261:129799.
42. Jayathilake PG, Jana S, Rushton S, Swales D, Bridgens B, Curtis T, Chen J. Extracellular polymeric substance production and aggregated bacteria colonization influence the competition of microbes in biofilms. *Front Microbiol*. 2017;8:1865.
43. Zhou Z, Li S, Wei G, Liu W, Zhang Y, Zhu C, et al. Cerium-based metal-Organic Framework with intrinsic haloperoxidase-like activity for Antibiofilm formation. *Adv Funct Mater*. 2022;32(39):2206294.
44. Giliopoulos D, Zamboulis A, Giannakoudakis D, Bikiaris D, Triantafyllidis K. Polymer/metal organic framework (MOF) nanocomposites for biomedical applications. *Molecules*. 2020;25(1):185.
45. Targhi AA, Moammeri A, Jamshidifar E, Abbaspour K, Sadeghi S, Lamakani L, Akbarzadeh I. Synergistic effect of curcumin-Cu and curcumin-Ag nanoparticle loaded niosome: enhanced antibacterial and anti-biofilm activities. *Bioorg Chem*. 2021;115:105116.
46. Neufeld BH, Neufeld MJ, Lutze A, Schweickart SM, Reynolds MM. Metal-organic framework material inhibits biofilm formation of *Pseudomonas aeruginosa*. *Adv Funct Mater*. 2017;27(34):1702255.
47. Zhou J, Guo M, Wu D, Shen M, Liu D, Ding T. Synthesis of UiO-66 loaded-caffeic acid and study of its antibacterial mechanism. *Food Chem*. 2023;402:134248.
48. Karakeçili A, Topuz B, Ersoy FŞ, Şahin T, Günyaktı A, Demirtaş TT. UiO-66 metal-organic framework as a double actor in chitosan scaffolds: antibiotic carrier and osteogenesis promoter. *Biomaterials Adv*. 2022;136:212757.
49. Tian F, Weng R, Huang X, Chen G, Huang Z. Fabrication of silver-doped UiO-66-NH2 and characterization of Antibacterial materials. *Coatings*. 2022;12(12):1939.

50. Lv H, Zhang Y, Chen P, Xue J, Jia X, Chen J. Enhanced synergistic antibacterial activity through a smart platform based on UiO-66 combined with photodynamic therapy and chemotherapy. *Langmuir*. 2020;36(15):4025–32.

Publisher's note

Springer Nature remains neutral with regard to jurisdictional claims in published maps and institutional affiliations.